Hierarchical Detection of Red Lesions in Retinal Images by Multiscale Correlation Filtering

Bob Zhang*[a], Xiangqian Wu[b,c], Jane You[c], Qin Li[c], Fakhri Karray[a]
[a]Dept. of Electrical and Computer Engineering University of Waterloo, Waterloo, ON, Canada;
[b]School of Computer Science and Technology, Harbin Institute of Technology, Harbin, P.R. China;
[c]Biometrics Research Center, Dept. of Computing, The Hong Kong Polytechnic University, Kowloon, Hong Kong

ABSTRACT

This paper presents an approach to the computer aided diagnosis (CAD) of diabetic retinopathy (DR) -- a common and severe complication of long-term diabetes which damages the retina and cause blindness. Since red lesions are regarded as the first signs of DR, there has been extensive research on effective detection and localization of these abnormalities in retinal images. In contrast to existing algorithms, a new approach based on Multiscale Correlation Filtering (MSCF) and dynamic thresholding is developed. This consists of two levels, Red Lesion Candidate Detection (coarse level) and True Red Lesion Detection (fine level). The approach was evaluated using data from Retinopathy On-line Challenge (ROC) competition website and we conclude our method to be effective and efficient.

Keywords: Computer-aided diagnosis (CAD), Diabetic Retinopathy (DR), Multiscale Correlation Filtering, red lesion detection

1. INTRODUCTION

Images of the ocular fundus, also known as retina images or retinal (fundus) images, can provide useful information about retinal [1], ophthalmic, and even systemic diseases such as diabetes [2-14], hypertension [15], glaucoma [16,17], obesity arteriosclerosis [18] and retinal artery occlusion. One such condition, diabetic retinopathy (DR), is the result of long-term diabetes and involves the formation on the retina of lesions which can lead to blindness.

In order to prevent the damage of this severe complication to a patient's vision, it is very important to diagnose diabetic retinopathy and provide appropriate treatment to minimize further deterioration as early as possible. It is also crucial to monitor the development of the disease by the detection and classification of changes in retinal images taken at different medical examinations to evaluate the effectiveness of the medical treatment and observe the evolution of the disease.

(a)

(b)

Fig. 1. Most common DR screening techniques (a) FA (Fluorescien Angiograms) and (b) color retinal image.

*yibo@pami.uwaterloo.ca; phone 1 519 888-4567 ext. 33746; fax 1 519 746-3077; pami.uwaterloo.ca

Medical Imaging 2009: Computer-Aided Diagnosis, edited by Nico Karssemeijer, Maryellen L. Giger
Proc. of SPIE Vol. 7260, 72601L · © 2009 SPIE · CCC code: 1605-7422/09/$18 · doi: 10.1117/12.813913

In general, DR can be classified into four stages: mild Non-Proliferative Diabetic Retinopathy (NPDR), moderate NPDR, severe NPDR, and Proliferative Diabetic Retinopathy (PDR). The damage caused by DR can be reduced and major vision loss [19,20] prevented if it is diagnosed and treated in its early stages. Thus, regular examination of diabetic patients' retina is very important. However, it is time consuming and subject to human errors if DR diagnosis is conducted by medical professionals manually. Therefore, automated or computer-aided analysis of diabetic patients' retina can help eye care specialist to screen larger populations of patients more accurately. An image processing approach provides a powerful tool in three aspects: image enhancement and feature extraction (feature based image registration), mass screening (diagnosis) and change detection, and classification (monitoring).

Fluorescien Angiograms (FA) is a medical estimation tool for screening DR [7-9,14]. FA injects fluorescein into the body before image capture so vessel features can standout. Although FA produces very clear gray-scale retinal images as seen in Fig. 1 (a) and is effective for describing hemorrhages and Neovascularization, it is not well-accepted by patients because of its intrusive nature. In [21], a method of staging DR using Transient Visual Evoked Potential (TVEP) was introduced. However, the procedure for generating a TVEP signal is complicated and time-consuming. Therefore, it is essential to develop a safe, easy, and comfortable method for screening DR. The analysis of color retinal images [3-6,13] displayed in Fig. 1 (b) is viewed as this feasible approach because the acquisition of retinal images is non- intrusive, very fast and easy. Processing of color retinal images is usually conducted in its green channel since red lesions have the highest contrast with its background here. This is illustrated in Fig. 2, which represents the image components in three different color bands -- Fig. 2 (a) is an original color retinal image, Fig. 2 (b), 2 (c) and 2 (d) represent component in red band (I_red), green band (I_green) and blue band (I_blue) respectively. In the green band objects such as blood vessels, lesions, the optic disc, etc., are most visible.

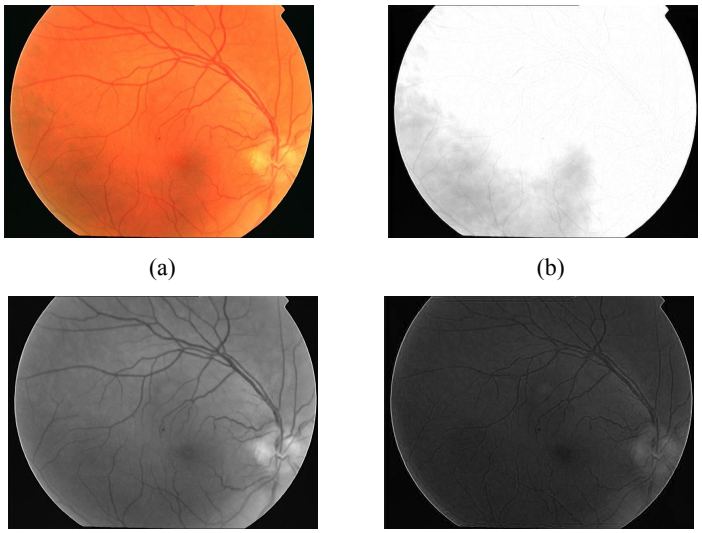

Fig. 2. The corresponding components in different color bands (a) the original color retinal image, (b) red band, (c) green band, and (d) blue band.

In [11], it was proposed to use artificial neural networks (ANNs) to automatically detect DR. The neural network consisted of an input pixel layer, hidden layer and output layer and was trained to recognize features such as blood vessels, exudates and hemorrhages. The images were divided into 30 x 30 and 20 x 20 squares pixels depending on the feature being detected and a trained observer then classified the squares as normal retina not showing blood vessels (normal), normal retina showing normal blood vessels (vessel), retina showing exudates (exudates), or retina showing hemorrhages or microaneurysms (hemorrhage). This method achieved a true positive rate of 88.4% and a true negative rate of 83.5%. Classification of hemorrhages was the most difficult part as their pixel values were similar to that of blood vessels. The system for diagnosing DR proposed in [12] detected blood vessels, the optic disk, the fovea (a pit in the retina that is full of ganglion cells and photoreceptors), and bright and dark lesions (both being abnormalities). Dark lesions included microaneurysms and hemorrhages while bright lesions included hard exudates and so-called cotton wool spots. Diagnosis is based on the number, type and location of abnormalities relative to the fovea. Two segments were partitioned from the original image, the fovea and the remaining portion of the retina. Abnormalities were found in

both segments by removing normal retinal features, which should leave either abnormalities and/or the background. The features extracted from the detected objects were then fed into a neural network to be classified as either normal or abnormal.

Although the above two methods are effective for some cases, they are subject to some limitations which include, microaneurysms are only classified but not extracted and the use of a neural network is time consuming. Niemeijer et. al. [13] overcame these problems and devised a way to detect/extract red lesions in fundus images based on candidate detection and classification. Candidate detection consisted of locating all possible red lesions by combining the Mathematical Morphology (Math Morph) method from [14] with pixel classification. The pixels were classified using a k-NN classifier with a reference standard that requires manually marking each image. The procedure then extracts 68 features from the remaining candidates, again using k-NN to classify them. This work reported a 100% true positive rate with an 87% false positive rate when deciding if an image has a red lesion. These are high true and false positive rates but this approach does not extract all possible lesions in an image and manual pixel classification in both [11,13] are laborious tasks that require medical experts, something not feasible when using larger numbers of images.

To avoid these problems, this paper presents a novel approach to the CAD of diabetic retinopathy that applies a hierarchical approach to the detection of red lesions in retinal images. The approach makes use of multiscale correlation filtering (MSCF) and dynamic thresholding for intensity-based detection and localization of red lesions in retinal images and has a two level hierarchical architecture. In the first level (coarse level), we detect candidate lesions using MSCF. In the second level (fine level), we detect true red lesions by extracting thirty one features from the level one candidates which are used to classify them. Fig. 3 shows the architecture of the proposed system.

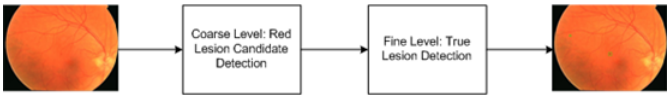

Fig. 3. System architecture of the proposed algorithm.

The remainder of this paper is organized as follows. Sections 2 and 3 describe the two level system architecture in detail. Section 4 presents and discusses the experimental results. Section 5 offers our conclusion and an outline of future work.

2. COARSE LEVEL: RED LESION CANDIDATE DETECTION

The task for course-level detection is to identify all of the possible red lesion candidates in a retinal image. Fig. 4 (a) and (b) show two lesions that were found in Fig. 1 (b) (shown in its green channel) and Fig. 4 (c) and (d) show their corresponding grayscale distributions. As can be seen, red lesions exhibit a Gaussian shape. This allows us to use a Gaussian function to detect lesions according to the similarity between the distributions of its grayscale.

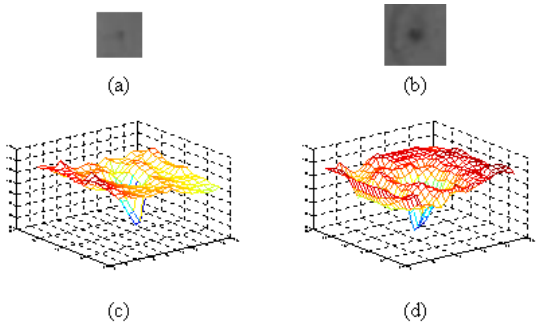

Fig. 4. The detection of red lesions in a color retinal image. (a) and (b) illustrate two red lesions found in a sample image shown in Fig. 2 (a). The corresponding mesh plots of (a) and (b) are shown in (c) and (d) respectively.

The Gaussian function can be defined as:

$$G(x,y) = \frac{1}{2\pi\sigma^2} e^{\frac{-x^2+y^2}{2\sigma^2}} \quad (1)$$

with its distribution shown in Fig. 5.

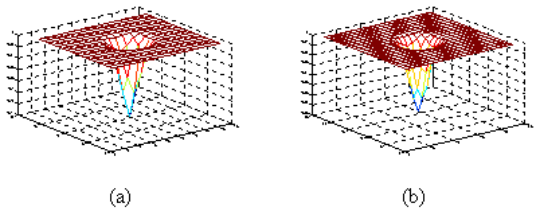

Fig. 5. The mesh plots of the Gaussian kernel with different scale factors. (a) scale factor σ=1.1 and (b) scale factor σ=1.5.

The correlation coefficient is a good way to measure the resemblance between the Gaussian function and grayscale distribution of lesions. If the two match, the correlation coefficient will be high and if they don't, the value will be low. The range of the coefficient is from 0 to 1.

The correlation function is defined as:

$$r = \frac{\sum_m \sum_n \left(A_{mn} - \overline{A}\right)\left(B_{mn} - \overline{B}\right)}{\sqrt{\left(\sum_m \sum_n \left(A_{mn} - \overline{A}\right)^2\right)\left(\sum_m \sum_n \left(B_{mn} - \overline{B}\right)^2\right)}} \tag{2}$$

where $\overline{A}$ and $\overline{B}$ are the mean.

Since lesions vary in size, different sigma values for the Gaussian kernel are required. For this purpose we include the selection of multiple scales in order to match various lesion dimensions. Fig. 6 (a, c and b, d) shows the responses and maximum correlation coefficients to different Gaussian kernels of the same two lesions depicted in Fig. 4. Images (a, c) on the left show the responses of Fig. 4 (a) to small and large kernels respectively. Images (b, d) on the right show the same thing but using Fig. 4 (b). From Fig. 6 it can be seen that applying one scale does not guarantee detection of the maximum coefficient as response Fig. 6 (a) has a greater coefficient using the smaller scale Gaussian kernel while response Fig. 6 (d) produces a higher coefficient using the larger scale kernel.

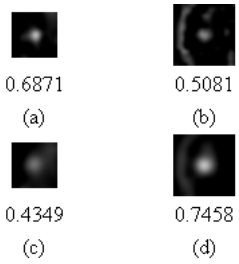

Fig. 6. The responses of lesions to different Gaussian kernels. (a) and (b) are responses for lesions in Fig. 4 (a) & (b) at a small scale, (c) and (d) are responses for lesions in Fig. 4 (a) & (b) at a larger scale respectively, where the maximum coefficient is placed below each responses.

The first step in coarse level candidate detection involves applying a non-linear filter with multiscale Gaussian kernels to the fundus image in order to calculate a correlation coefficient for each pixel.

Because red lesions are circular, the Gaussian kernels are also circular as this will ensure that the response (a correlation coefficient) will be high. Based on extensive experimentation, we chose five scales for the kernel to represent microaneurysms of different sizes with the sigma of the Gaussian function being 1.1, 1.2, 1.3, 1.4 and 1.5. The maximum coefficients from each of the five responses were combined to form a final response. Figure 7 depicts the final response, where Fig. 7 (a) is an input retinal image and Fig. 7 (b) is the output. The brighter spots seen in Fig. 7 (b) have a higher coefficient and therefore are more likely to be true lesions.

A threshold is next applied in order to determine the number of lesion candidates. Application of a threshold creates a binary image as in the example in Fig. 8, where the threshold value was set to 0.4 in order to segment Fig. 7. Since red lesions cannot occur on blood vessels, an adaptive thresholding technique is used to first locate these vessels and remove any spots on them, thereby reducing the number of candidates. Figure 9 shows a vascular map, where Fig. 9 (a) is an original image, Fig. 9 (b) is the output of the corresponding vascular map with all the blood vessels that were detected after adaptive thresholding. Any candidates on these vessels are removed from Fig. 8 and the result can be seen in Fig. 10.

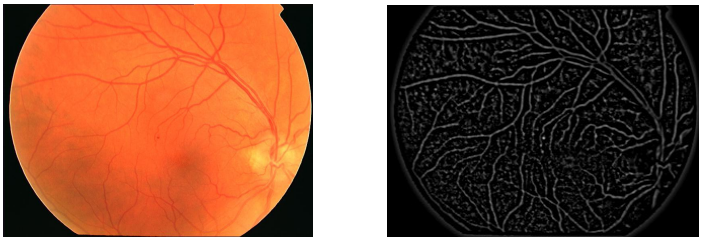

(a) (b)

Fig. 7. The final response of a testing image (a) the input retinal image (b) the output.

Fig. 8. Result after segmenting Fig. 7 with a threshold of 0.4. The white spots marked are possible red lesions.

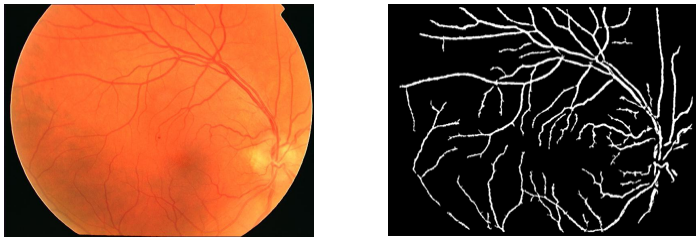

(a) (b)

Fig. 9. The vascular map of a retinal image. (a) the sample image given in Fig. 1 (b) and (b) the output of its vascular map.

Fig. 10. The remaining candidates from Fig. 8 after candidates on the blood vessels were removed.

The candidate lesions that remain in Fig. 10 at this point do not represent the true lesion size, so we apply region growing based on [13]. We first calculate the grayscale intensity pixel value(s) for each candidate (i_green for I_green

and i_bg for I_bg). I_bg is the background of I_green and is computed by applying a median filter of size 25 x 25 to I_green. The lowest intensity in i_green (I_darkest) is also required. These values are used to find a threshold *t* where:

$$t = I\_darkest - x(I\_darkest - i\_bg) \quad (3)$$

In this paper, *x* is set to 0.5. The value *t* is then used to segment I_green into a binary image where region growing begins from the pixel having the intensity I_darkest and terminates when no more pixels are connected to it. If the resultant region is greater than 120 pixels it's discarded as no true lesion can be that large. Fig. 11 shows the result of region growing for the candidates in Fig. 10.

Fig. 11. Result of region growing for the candidates in Fig. 10.

3. FINE LEVEL: TRUE LESION DETECTION

The task for fine level lesion detection is to detect true red lesions in the candidate set, which can be implemented through feature extraction. We used a total of 31 features for each candidate, based on shape, grayscale pixel intensity, color intensity, responses of Gaussian filter-banks, and correlation coefficient values. The following lists the 31 features used to discriminate red lesions in our proposed approach. Features 27-29 are unique to the proposed method as it is based on the correlation coefficient of each pixel, calculated beforehand. The last two features, major and minor axis length are added to diversify the already existing shape features.

1. The area *a* of the candidate. Lesions have a small area compared to other objects in the retina.
2. The perimeter *p* of the candidate. Lesions have a small perimeter compared to other objects in the retina.
3. The aspect ratio $r = l / w$ where *l* and *w* are the major and minor axis lengths of the candidate. For a true lesion its major and minor axis should be quite similar.
4. The circularity $c = 4\pi a / p^2$. True lesions are circular in shape.
5. The total intensity *i_green* of the candidate in I_green. True lesions have higher intensities.
6. The total intensity *i_sc* of the candidate in I_SC.
7. The average intensity of i_green, $m\_green = i\_green / a$.
8. The average intensity of i_sc, $m\_sc = i\_sc / a$.
9. The normalized intensity in I_green, $NI\_green = (1/\sigma)(i\_green - x)$ where σ and *x* are the standard deviation and mean pixel value of I_bg.
10. The normalized intensity in I_SC, $NI\_SC = (1/\sigma)(i\_sc - x)$.
11. The normalized average intensity in I_green, $NM\_green = (1/\sigma)(m\_green - x)$.
12. The normalized average intensity in I_SC, $NM\_sc = (1/\sigma)(m\_sc - x)$.
13. The intensity of *I_darkest* in I_match.

14. The compactness $v = \sqrt{\sum (d_i - d)^2 / n}$ where d_i is the distance of each boundary pixel of the candidate to its center, d is the mean of all these distances and n is the number of boundary pixels. True lesions are compact.
15. The difference between the average pixel values of the candidate and a circular region centered on it in the red channel (RGB color space). The circular region is calculated by dilating the candidate with a disk of radius 6. Since lesions have a Gaussian distribution when examining its grayscale values, the contrast of the lesion with its background should be high.
16. Repeat feature 15 but in the green channel, blue channel and hue channel from the HSI color space. (3 features)
17. The average Gaussian filter response of I_green with σ=1, 2, 4 and 8. (4 features)
18. The standard deviation response of I_green after Gaussian filtering with σ=1, 2, 4 and 8. (4 features)
19. The maximum, minimum and average correlation coefficient of the candidate. Candidates with a higher coefficient are more likely to be true lesions. (3 features)
20. The major axis length of the candidate. Generally, lesions do not have a significant major nor minor axis length.
21. The minor axis length of the candidate.

(a) (b) (c)

Fig. 12. The output of red lesion detection. (a) the original retinal image (b) the output of coarse – level detection (c) the final output of fine – level detection where the colored spot inside the green squares mark the approximate location of the detected lesions using the proposed algorithm.

After features are extracted from the candidates, we divide them into two groups: true lesions and false lesions (how we do this is explained in Section 4). We then obtain the minimum and maximum values of each feature in the true lesion group and store them in a discrimination table as in Table 1. The 31 features are given a number and the min. and max. values for that feature can be read off in the columns. This table can be used to eliminate any candidates whose features are greater than max or less than min. For feature 16 which computes the contrast of the candidates and its surrounding area in the green channel, the min. value was manually set to 8. By manually setting this value to be higher than the actual min. of feature 16, some true and many false lesions are removed. This feature was specifically chosen since the contrast between lesions and its surrounding background are known to be high. The remaining candidates whose feature values are between min. and max. are the final detected red lesions. We applied this table to the candidates drawn from Fig. 11 and obtained the result in Fig. 12. The true candidates are then mapped back to the original image to show the location of true lesions (inside the green squares, shown in Fig. 12 (c)). As can be seen, a significant number of candidates have been removed (from Fig. 12 (b)). For the final output image given in Fig. 12 (c), all true lesions were detected with no false positives.

Table 1. The discrimination table of different retinal features.

Feature Number	Min.	Max.	Feature Number	Min.	Max.	Feature Number	Min.	Max.
1	2	109	12	0.164831	5.08576	23	36.00843	182.7637
2	2	113.0122	13	7	255	24	0.003416	3.00799
3	1	5.618986	14	0	3.743681	25	37.95791	183.7483
4	0.090521	6.283185	15	-31.368	2.863946	26	0.009462	1.797795
5	58	10676	16	8	35.37533	27	0.106603	0.785072
6	338	19451	17	-27.1471	6.368521	28	0	0.547187
7	25.17241	177.0417	18	-0.01944	0.002723	29	0.053335	0.658546
8	104.8125	221.9348	19	27.66061	179.0988	30	2.309401	29.53404
9	-0.31038	203.8908	20	0.01962	8.292589	31	1.154701	14.09998
10	6.138524	448.9355	21	30.81245	180.773			
11	-1.15234	0.921628	22	0.044188	6.747434			

4. EXPERIMENTAL RESULTS AND ANALYSIS

To evaluate our proposed algorithm, we conducted a sequence of experiments on 100 images (split into 50 training and 50 test) in the public retinal image database provided on the ROC competition website [22]. The images were all taken with Topcon NW 100, NW 200 or Canon CR5-45NM 'non-mydriatic' cameras at the default resolution and compression settings from patients with diabetes without known diabetic retinopathy (at the moment of photography). The images are a random sample of all patients that were noted to have 'red lesions' from a large (> 10,000 patients) diabetic retinopathy screening program, and each image is from a different patient. All images are in JPEG compressed format with sizes 768 x 576, 1058 x 1061, 1062 x 1061, 1379 x 1383, 1381 x 1385, 1385 x 1382, 1386 x 1384, 1389 x 1383, 1389 x 1391 and 1394 x 1392 pixels. Each image comes with a reference standard that marks every lesion agreed upon by the consensus of 4 experts. This reference standard helps identify true lesions used in the discrimination table. Some images contained so-called 'don't care' objects where a consensus could not be reached or where the objects are not microaneurysms (e.g. hemorrhages, pigment spots, etc.). We applied the proposed algorithm on all images and did not consider or use the 'don't care' objects. To segment the final response after applying the kernel functions we used threshold values ranging from 0.1 to 1.0, each time building a discrimination table according to the true red lesion feature values and using it to remove some candidates. We compared our algorithm with Math Morph [14]. This was done by first implementing [14] and then testing with the same data as the proposed algorithm. We were not able to compare it to [13] since the reference standard provided did not label each pixel as required by this method.

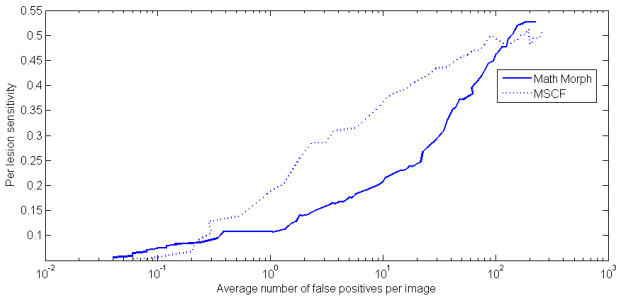

Fig. 13. Plot of FROC comparing MSCF (dotted curve) with Math Morph (solid curve) on the training data.

The performance of our hierarchical approach based on MSCF for red lesion detection is evaluated by plotting sensitivity against the average number of false positives per image (FROC) using the 50 training images, shown in Fig. 13 as a dotted curve. Sensitivity is the number of true lesions detected while false positive is the number of non lesions detected as true lesions. Please note that the horizontal axis is in logarithmic scale. The FROC plot also contains a solid curve, which is our implementation of Math Morph. As can be seen the majority of the dotted curve has a higher sensitivity compared with the solid curve for the same false positives per image. Table 2 lists the sensitivity of 0.1, 0.2, 0.4, 0.8, 1.6, 3.2 and 6.4 false positives per image of both methods derived from Fig. 13. In this table the proposed method has a greater sensitivity from 0.4 to 6.4 with the average of all seven points being 0.1856 and 0.1232 for Math Morph.

Table 2. The average number of false positives per image for training data.

False Positive Rate	MSCF	Math Morph
0.1	0.0565	0.0744
0.2	0.0685	0.0851
0.4	0.1335	0.1072
0.8	0.1707	0.1072
1.6	0.2536	0.1400
3.2	0.2917	0.1600
6.4	0.3250	0.1885
Average	0.1856	0.1232

Results based on the 50 test images are displayed in Fig. 14, also in the form of a FROC plot. Again, the dotted line represents MSCF while the solid line is Math Morph. The same trend found in Fig. 13 applies to Fig. 14 where the majority of MSCF points are higher than Math Morph. Table 3 which measures the same false positives per image as Table 2 except for the test data supports this calm, as the sensitivity of MSCF is greater than Math Morph with the average sensitivity being 0.3739 – MSCF and 0.0876 – Math Morph. This clearly demonstrates that MSCF outperforms Math Morph. The remaining true lesions not detected were due to the quality of the images, the selection of sigma for the Gaussian filter, the location of the lesions being too close to blood vessels and little contrast between the lesions and its surrounding background.

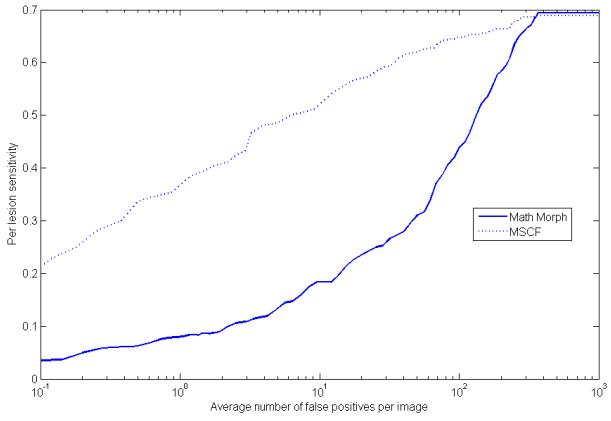

Fig. 14. Plot of FROC comparing MSCF (dotted curve) with Math Morph (solid curve) on the test data.

Table 3. The average number of false positives per image for test data.

False Positive Rate	MSCF	Math Morph
0.1	0.2296	0.0361
0.2	0.2810	0.0556
0.4	0.3361	0.0630
0.8	0.3744	0.0799
1.6	0.4081	0.0919
3.2	0.4808	0.1182
6.4	0.5071	0.1683
Average	0.3739	0.0876

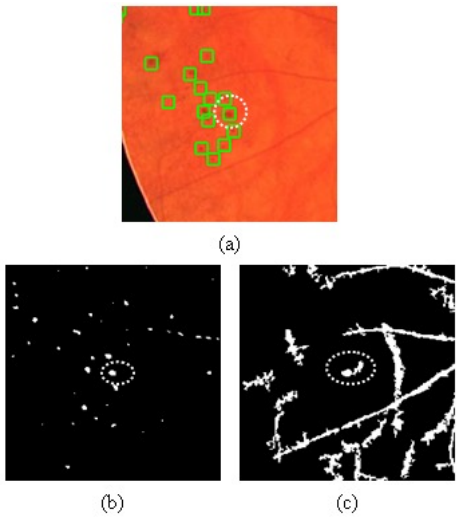

Fig. 15. True lesion being recognized as part of the blood vessel. (a) A cropped retinal image marked with true lesions. (b) candidates lesions detected in (a). (c) Vascular map of (a). The central lesion, enclosed with dashes in (a) and (b) is detected as part of the blood vessel in (c).

The experiments raise four particular issues which require further consideration. First, there is the quality of the images, which are JPEG compressed and therefore some of the lesions are too small or too blurred to be seen with the naked eye. Second there is the choice of scales for the Gaussian kernel. The use of only small scales means that larger lesions will not be extracted because the smaller kernel cannot cover/match the larger spots and thereby produces a lower correlation coefficient. The same problem arises when using a larger scale to cover/match a small lesion. If such candidate lesions are not detected after the coarse level, they will be lost forever. Third, a few lesions located next to or nearby blood vessels are removed in the coarse level. This is because these lesions are recognized as part of the vascular map and therefore are removed along with real vessels. Figure 15 illustrates this problem where Fig. 15 (a) is a cropped color retinal image with marked (green squares) lesions, Fig. 15 (b) are candidates detected from Fig. 15 (a) and Fig. 15 (c) is the vascular map of Fig. 15 (a). The central lesion (enclosed in dashes) in Fig. 15 (a) is detected as seen in Fig. 15 (b) but also appears as a vessel in Fig. 15 (c). This subsequently removes it as a candidate from Fig. 15 (b) in the next step of the coarse level.

A fourth issue for further consideration relates to the effect of contrast on true and false detected lesions. When true lesions have a low contrast with its background, as can be seen in the examples in Fig. 16, the lesions will not exhibit a

Gaussian shape and it becomes difficult for the Gaussian kernels to produce a high correlation coefficient (see Table 4 (left)). From our results several of the spots detected as false lesions are circular in shape and have significant contrast with its background which explains its high correlation coefficient. Of these, some are possibly lesions (where a consensus was not reached by the 4 experts). Fig. 17 shows four examples of these contentious spots with Table 4 (right) displaying their correlation coefficients. We deem these objects reasonable to be detected as they resemble true red lesions.

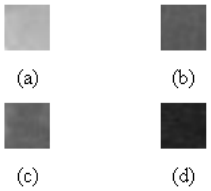

Fig. 16. True lesions with low contrast.

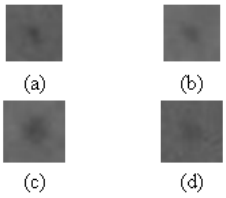

Fig. 17. False positive lesion candidates with high contrast.

Table 4. True lesions with low intensity contrast (left) and false positive candidates that resemble true lesions (right).

True Lesion	Max. response
Fig. 16 (a)	0.1696
Fig. 16 (b)	0.1624
Fig. 16 (c)	0.1934
Fig. 16 (d)	0.1715

False Lesion	Max. response
Fig. 17 (a)	0.7527
Fig. 17 (b)	0.7235
Fig. 17 (c)	0.6564
Fig. 17 (d)	0.6269

5. CONCLUSION AND FUTURE WORK

In this paper we proposed a hierarchical approach based on multiscale correlation filtering (MSCF) to detect all red lesions from a color retinal image. This consisted of Coarse Level: Red Lesion Candidate Detection using MSCF and Fine Level: True Red Lesion Detection. The approach was evaluated using the public retinal image database provided on the ROC competition website and conclude that the proposed approach is effective and efficient for intensity-based red lesion detection and localization for DR diagnosis. The selection of scales in the first level is vital to the success of succeeding steps. Sigma values have to be chosen such that the kernel can match lesions of various sizes always producing a high correlation coefficient. Currently only five scales are used. If more scales specifically designed to match small and large lesions are implemented and then combined to form a scale production, this might improve the existing results. Further improvement of the proposed algorithm is to develop an automatic scale selection scheme which can determine the best scale for the system based on the training set.

REFERENCES

[1] Goldbaum, M., Moezzi, S., Taylor, A., Chatterjee, S., Boyd, J., Hunter, E. and Jain, R., "Automated diagnosis and image understanding with object extraction, object classification, and inferencing in retinal images," Proc. IEEE International Conference on Image Processing, 695–698 (1996).

[2] Cree, M., Olson, J., McHardy, K., Sharp, P. and Forrester, J., "A fully automated comparative microaneurysm digital detection system," Eye 11, 622–628 (1997).

[3] Hipwell, J., Strachant, F., Olson, J., McHardy, K., Sharp, P. and Forrester, J., "Automated detection of microaneurysms in digital red-free photographs: a diabetic retinopathy screening tool," Diabetic Med. 17(8), 588–594 (2000).

[4] Larsen, M., Godt, J., Larsen, N., Lund-Andersen, H., Sjølie, A., Agardh, E., Kalm, H., Grunkin, M. and Owens, D., "Automated detection of fundus photographic red lesions in diabetic retinopathy," Investigat. Ophthalmol. Vis. Sci. 44(2), 761–766 (2003).

[5] Walter, T., Klein, J. C., Massin, P. and Erginay, A., "A contribution of image processing to the diagnosis of diabetic retinopathy—detection of exudates in color fundus images of the human retina," IEEE Trans. Med. Imag. 21(10), 1236–1243 (2002).

[6] Sinthanayothin, C., Boyce, J. F., Williamson, T. H., Cook, H. L., Mensah, E., Lal, S. and Usher, D., "Automated detection of diabetic retinopathy on digital fundus images," Diabetic Med. 19(2), 105–112 (2002).

[7] Frame, A. J., Undill, P. E., Cree, M. J., Olson, J. A., McHardy, K. C., Sharp, P. F. and Forrester, J. F., "A comparison of computer based classification methods applied to the detection of microaneurysms in opthalmic fluorescein angiograms," Computers in Biomedical Research 28(3), 225–238 (1998).

[8] Mendonca, A. M., Campilho, A. J. and Nunes, J. M., "Automatic segmentation of microaneurysms in retinal angiograms of diabetic patients," Proc. IEEE International Conference of Image Analysis Applications, 728–733 (1996).

[9] Spencer, T., Phillips, R. P., Sharp, P. F. and Forrester, J. V., "Automated detection and quantification of microaneurysms in fluorescein angiograms," Graefe's Archive for Clinical and Experimental Ophthalmology 230(1), 36–41 (1992).

[10] Sinthanayothin, C., Kongbunkiat, V., Phoojaruenchanachai, S. and Singalavanija, A., "Automated screening system for diabetic retinopathy," Proc. IEEE Image and Signal Processing and Analysis, 915–920 (2003).

[11] Gardner, G. G., Keating, D., Williamson, T. H. and Elliott, A. T., "Automatic detection of diabetic retinopathy using an artificial neural network: a screening tool," Brit. J. Ophthalmol. 80(11), 940–944 (1996).

[12] Estabridis, K. and de Figueiredo, R. J. P., "Automatic Detection and Diagnosis of Diabetic Retinopathy," Proc. IEEE International Conference on Image Processing, 445–448 (2007).

[13] Niemeijer, M., van Ginneken, B., Staal, J., Suttorp-Schulten, M. S. A. and Abramoff, M. D., "Automatic detection of red lesions in digital color fundus photographs," IEEE Trans. Medical Imaging 24(5), 584–592 (2005).

[14] Spencer, T., Olson, J. A., McHardy, K. C., Sharp, P. F. and Forrester, J. V., "An image-processing strategy for the segmentation of microaneurysms in fluorescein angiograms of the ocular fundus," Computers and Biomedical Research 29(4), 284-302 (1996).

[15] Leung, H., Wang, J. J., Rochtchina, E., Wong, T. Y., Klein, R. and Mitchell, P., "Impact of current and past blood pressure on retinal arteriolar diameter in older population," J. Hypertens. 22(8), 1543–1549 (2004).

[16] Mitchell, P., Leung, H., Wang, J. J., Rochtchina, E., Lee, A. J., Wong, T. Y. and Klein, R., "Retinal vessel diameter and open-angle glaucoma: the Blue Mountains eye study," Ophthalmology 112(2), 245–250 (2005).

[17] Chrástek, R., Wolf, M., Donath, K., Niemann, H., Paulus, D., Hothorn, T., Lausen, B., Lämmer, L., Mardin, C. Y. and Michelson, G., "Automated segmentation of the optic nerve head for diagnosis of glaucoma," IEEE Trans. Medical Image Analysis 9(4), 297–314 (2005).

[18] Wang, J. J., Taylor, B., Wong, T. Y., Chua, B., Rochtchina, E., Klein, R. and Mitchell, P., "Retinal vessel diameters and obesity: a population-based study in older persons," Obes. Res. 14(2), 206–214 (2006).

[19] Taylor, H. R., and Keeffe, J. E., "World blindness: A 21st century perspective," Brit. J. Ophthalmol. 85(3), 261–266 (2001).

[20] Klein, R., Meuer, S. M., Moss, S. E. and Klein, B. E., "Retinal microaneurysm counts and 10-year progression of diabetic retinopathy," Archives of Ophthalmology 113(11), 1386–1391 (1995).

[21] Sivakumar, R., "Staging of Diabetic Retinopathy using TVEP Phase Spectral Periodicity Analysis," Proc. IEEE International Conference on Engineering of Intelligent Systems, 1–5 (2006).

[22] Retinopathy Online Challenge, http://roc.healthcare.uiowa.edu/ (2008).